DOI: 10.1002/((please add manuscript number))

Article type: Communication

Giant Ferroelectric Polarization in Ultrathin Ferroelectrics via Boundary-condition Engineering

*Lin Xie, Linze Li, Colin A. Heikes, Yi Zhang, Zijian Hong, Peng Gao, Christopher T. Nelson, Fei Xue, Emmanouil Kioupakis, Longqing Chen, Darrel G. Schlom, Peng Wang, Xiaoqing Pan**

Dr. L. Xie, Dr. L. Z. Li, Dr. Y. Zhang, Prof. X. Q. Pan

Department of Chemical Engineering and Materials Science, University of California Irvine, Irvine, CA 92697, USA

E-mail: xiaoqinp@uci.edu

[+] L.X. and L.Z.L. contributed equally to this work.

Dr. L. Xie, Prof. P. Wang

National Laboratory of Solid State Microstructures and College of Engineering and Applied Sciences, Nanjing University, Nanjing, Jiangsu 210093, People's Republic of China

Dr. C. A. Heikes, Prof. D. G. Schlom

Department of Materials Science and Engineering, Cornell University, Ithaca, NY 14850, USA

Dr. P. Gao, Dr. C.T. Nelson, Prof. E. Kioupakis

Department of Materials Science and Engineering, University of Michigan, Ann Arbor, MI 48105, USA

Dr. Z. J. Hong, Dr. F. Xue, Prof. L.-Q. Chen

Department of Materials Science and Engineering, Pennsylvania State University, State College, PA 16802, USA

Keywords: ultrathin ferroelectric film, polarization, surface effect, scanning transmission electron microscopy

Tailoring and enhancing the functional properties of materials at reduced dimension is critical for continuous advancements of modern electronic devices. Here, we report the discovery of local surface induced giant spontaneous polarization in ultrathin $BiFeO_3$ ferroelectric films. Using aberration-corrected scanning transmission electron microscopy (STEM), it is found that the spontaneous polarization in a 2 nm thick ultrathin $BiFeO_3$ film is abnormally increased up to ~90-100 $\mu C/cm^2$ in the out-of-plane direction and a pecuiliar rumpled nanodomain structure with very large variation in *c*/*a* ratios, which is in analog to morphotropic phase boundaries (MPB), is formed. By a combination of density functional and phase-field calculations, it's shown that it's the unique single atomic Bi_2O_{3-x} layer at the surface that leads to the enhanced polarization and appearance of MPB-like nanodomain structure. This finding clearly demonstrates a novel route to the enhanced functional properties in the material system with reduced dimension via engineering the surface boundary conditions.

The integration of ferroelectric thin films into electronic devices has led to an upsurge of interest in exploring novel devices with exotic physical properties, owing to the multitude of functionality of ferroelectrics[1–3]. A number of applications, e.g. high-density nonvolatile random access memories[4] and prototype devices in electronics, optoelectronics and electro-mechanics, have been proposed based on the coupling between the ferroelectric polarization and other functional properties, i.e. mechanical, optical and magnetic properties of ferroelectric materials[2,5–7]. However, as the size of the device with ferroelectrics is reduced to the scale required for practical industrial semiconductor devices, this development is challenged by the long-standing issue concerning the 'dead layer' or size scaling effect, where ferroelectric polarization in the films with a thickness down to a few nanometers is hampered due to the strong depolarizing electric field, which arises from the incomplete screening at the surface or interface[8–10]. On the other hand, several experimental works indicated that the spontaneous polarization in a ferroelectric thin film could be retained down to the thickness of only several unitcells[7,11–14], but with reduced transition temperature[11] and polarization[13]. Therefore, given the thriving practical industrial application of nanoelectronic devices, it's of great importance to pursue enhanced ferroelectric properties at the reduced dimension. Using atomistic simulations, it was demonstrated that an overall enhancement of ferroelectricity can be produced in ultrathin ferroelectric capacitors by controlling the chemical environments at the metal/oxide interfaces[15]. Recent experimental work suggested that a reduction in size to a scale of a few nanometers can lead to the emergence of weak room-temperature ferroelectricity in an otherwise non-ferroelectric $SrTiO_3$ film, a result of electrically induced alignment of polar nano-regions due to Sr

vacancies[16]. However, a direct experimental observation of enhanced polarizations at reduced dimensions in common ferroelectrics has not yet been deterministically identified. In this study, a 2 nm thick ultrathin BFO film was prepared, and its structural properties were investigated to demonstrate that a prominent enhancement of ferroelectric polarization and the formation of MPB-like domain structure can be achieved by changing the surface boundary condition through single atomic Bi_2O_{3-x} layers.

The films studied in this paper are epitaxially grown on $TbScO_3$ (TSO) $(1\,\bar{1}0)_O$ substrates by molecular-beam epitaxy; the growth direction for BFO is $[001]_{PC}$ (the subscripts O and PC stand for orthorhombic and pseudocubic indices, respectively). At ambient conditions, a BFO/TSO $(1\,\bar{1}0)_O$ thin film is typically of rhombohedral(*R*) phase, with its spontaneous polarization $\mathbf{P}_S$ (~90 μC/cm^2) pointing in one of the symmetrically equivalent $<111>_{PC}$ directions (**Figure 1a**)[17,18]. The ultrathin film was characterized by STEM high-angle annular dark field (HAADF) imaging and **Figure 1b** shows the atomic-resolution image viewed along the $[100]_{PC}$ direction. Note that the film has two remarkable structural features. First, unlike conventional epitaxial thin films with flat surface, the film is not homogeneous in terms of its out-of-plane lattice, but characterized by a peculiar periodic rumpled structure. This rumpling essentially takes the form of periodic lattice dilations along the film's growth direction, i.e. $[001]_{PC}$. Second, as indicated by the yellow arrows, there also exist unique structures on the film's surface. These particular surface structures are discontinuous and only one single atomic layer in thickness (see the inset of Figure 1b for a better view of the surface structure). Their reduced image contrast with respect to the film are probably due to the discontinuous distribution of these monolayers along the beam direction as well (see Supporting Information for

details). As shall be shown below, these two structural features are closely associated with each other and give rise to a large enhancement in the ferroelectric polarizations.

The rumpling structure and ferroelectricity of the film are characterized by measuring the relative displacements of *B*-site Fe atoms $\mathbf{D}_{\mathrm{FB}}$ with respect to the center of four surrounding *A*-site Bi atoms[19,20]. Local ferroelectric polarization $\mathbf{P}_{\mathrm{S}}$ is related to $\mathbf{D}_{\mathrm{FB}}$ as $\mathbf{P}_{\mathrm{S}} \propto -\mathbf{D}_{\mathrm{FB}}$ since, in general, the relative displacement of the Fe atom is in the opposite direction of the polarization. **Figure 2a** shows the map of the local Fe displacements and clearly illustrates the local ferroelectric polarization and domain structure. Unlike the conventional *R*-phase BFO (shown in Figure 1a), the domain structure of the film is similar to those expected for the mixture of tetragonal (*T*) phase and *R*-phase ferroelectrics and closely resemble the 'morphotropic phase boundary' found in $Pb(Zr_{0.5}Ti_{0.5})O_3$[21]. Here the 'morphotropic' term is used to refer to the different symmetry of the domains. In the following text, we will denote the domains with large out-of-plane component as *c*-type domains, while those with attenuated polarization are denoted as *a*-type domains. The alternating *c*-/*a*-type domain structures and lattice dilations can be seen more clearly in the maps of the out-of-plane displacement $-D_{\mathrm{FB}}^{(z)}$ (**Figure 2b**) and the *c*/*a* ratios (**Figure 2c**). Note that there is a perfect one-to-one match between the domains and the appearance of the surface monolayer, where the single atomic layer appears exclusively on top of the *c*-type domains.

Careful analysis of the *c*/*a* ratios, $\left|\mathbf{D}_{\mathrm{FB}}\right|$ and $-D_{\mathrm{FB}}^{(z)}$ of these two types of domains is given in **Figure 2d**, **2e** and **2f**. At the interface, the *c*/*a* ratios of both *c*-type and *a*-type domains are close to the bulk value (~1.0). The *c*/*a* ratio of *c*-type domains monotonically increases from the interface to the surface, while that of *a*-type domains seems relatively uniform through the film. At the top

surface, the *c*/*a* ratio of *c*-type domains reaches up to a value of ~1.15. Meanwhile, the ferroelectric displacements $|\mathbf{D}_{\mathrm{FB}}|$ and $-D_{\mathrm{FB}}^{(z)}$ of *c*-type domains behave in a similar manner to their *c*/*a* ratios. At the interface, $|\mathbf{D}_{\mathrm{FB}}|$ of *c*-type domains (~0.28±0.05 Å) is comparable to the bulk value ~0.33 Å. At the top surface of the film, $|\mathbf{D}_{\mathrm{FB}}|$ increases dramatically to a value of ~0.5±0.08 Å, nearly 30% greater than the bulk value. The corresponding $-D_{\mathrm{FB}}^{(z)}$ is also markedly enhanced to ~0.4±0.02 Å. To estimate the resulting polarization, we assume that $\mathbf{P}_{\mathrm{S}}$ is proportional to $\mathbf{D}_{\mathrm{FB}}$[19] and given a polarization of ~90 μC/cm^2 for $|\mathbf{D}_{\mathrm{FB}}|$=0.33 Å, a giant polarization of ~136 μC/cm^2 is obtained for $|\mathbf{D}_{\mathrm{FB}}|$=0.5 Å. Similarly, the out-of-plane polarization is estimated to be ~109 μC/cm^2 for $-D_{\mathrm{FB}}^{(z)}$=0.4 Å. In comparison, the out-of-plane polarization of *a*-type domains is significantly suppressed, and $-D_{\mathrm{FB}}^{(z)}$ is only about ~0.05-0.13(±0.07) Å, much smaller than its bulk counterpart. Using the same approximation, the polarization is estimated to be only about ~14-35(±19) μC/cm^2. While the suppression of polarization due to the presence of a depolarizing field is expected in ultrathin ferroelectric films, an anomalous polarization enhancement up to ~136 μC/cm^2 is very surprising. This value is even comparable to that of super-tetragonal BFO films, in which a polarization up to ~150 μC/cm^2 can be induced by a large compressive epitaxial strain[22]. More importantly, according to conventional understanding of ferroelectric polarization in ultrathin films, its spontaneous polarization is expected to be substantially suppressed by the surface and the depolarizing field[8,9]. Our results for the first time clearly demonstrate that ferroelectricity can be prominently enhanced and novel MPB-like domain structure can form in an ultrathin ferroelectric film by changing the surface condition.

The driving force of the as-observed enhanced polarization, as well as the large lattice dilations, cannot be simply explained by the epitaxial strain applied by the substrate (the lattice mismatch between BFO and TSO is < 0.14%)[19,23] and should have other explanation. The one-to-one correspondence between the appearance of the *c*-type domains with enhanced polarization and the surface monolayers might be a possible mechanism. In fact, it was found that a parasitic bismuth compound in BFO could lead to a tetragonal BFO phase with a giant *c*/*a* ratio[24], which suggest that the abnormally enhanced polarization and *c*/*a* ratios might be related to the surface monolayers. In order to gain deeper insights into the underlying physics of the enhanced ferroelectric and the surface monolayer, we carry out further chemical analysis of the surface structure. As is shown in the inset of Figure 1b, the single atomic layer does not comply with the *ABAB* (*A* – BiO plane, *B* – FeO_2 plane) stacking order of BFO. Instead, the atoms are shifted with respect to the lower BiO planes and result in a characteristic zigzag-like structure. The chemical composition of the surface layers was investigated via electron energy-loss spectroscopy (EELS) line scans from the substrate to the surface (see Methods for details of EELS experiments). Six individual spectra, five for the BFO film and one for the single atomic surface layer, are extracted from the line scan profile and the processed spectra are displayed in **Figure 3**. While the lower five spectra of the BFO film all show the elemental O-K (~530 eV) and Fe-$L_{2,3}$ (~708 eV) energy-loss peaks, the surface layers are deficient in Fe. Meanwhile, the proportion of O changes much less. Direct evidence of Bi in the surface monolayer is difficult to obtain straightforwardly from EELS due to its extremely high energy-loss (~2580 eV). But provided that the HAADF image contrast of the surface layers is similar to that of the film, it is strongly inferred that the surface layer is primarily a compound of Bi and O, and the most probable candidate is nonstoichiometric Bi_2O_{3-x}. In fact, Bi_2O_{3-x} has a relatively small lattice mismatch

with BFO[25] and its structure (**Figure S1**) is also in reasonably good agreement with the characteristic zigzag-like structure discovered in the HAADF images. The formation of such surface monolayers is possibly due to certain surface reconstruction or relaxation processes[26,27]. Another plausible explanation is that these atomic layers originate from an outward migration of the lower BiO planes due to the volatility of Bi. It should also be noted that similar structure with elongated lattice parameters occur in the form of antiphase boundary in doped BFO[28,29], which suggests that these surface monolayers might be nucleation sites during growth. If more FeO_2 is added, this transient state would become proper BFO. In fact, such an implication is supported by a sequence of films grown at different thickness, in which the same surface structure can be observed (see Supporting Information for the discussions of the surface structure, **Figure S2-S3**, and experimental results of films with different thickness, **Figure S4-S5**). Nonetheless, these structures are directly associated with the *c*-type domains and possibly a dominant factor in the enhanced ferroelectricity.

DFT calculations were carried out to corroborate the proposed surface enhanced polarization mechanism. In the calculation, a single Bi_2O_3 layer was placed on top of BFO and a full structural relaxation was performed (see Supporting Information for details of calculation). **Figure 4a** displays the atomic structure after the relaxation, and the lattice dilation can be readily observed at the top BFO layer. The calculated *c*/*a* ratio and $\left|\mathbf{D}_{\mathrm{FB}}\right|$ are summarized in **Figure 4b** and they match the experimental values very well. First, the *c*/*a* ratio increases monotonically along the $[001]_{PC}$ direction, starting from ~1.0 at the interface and reaching a value of ~1.2 at the surface. Second, the calculated $\left|\mathbf{D}_{\mathrm{FB}}\right|$ at the interface is ~0.33 Å and increases substantially to a value of ~0.58 Å at the top surface. Local polarization was then calculated from the relaxed structure. According to modern theory of polarization[30,31], the polarization $\mathbf{P}_i$ of unit cell i is[32]:

$$\mathbf{P}_i = \frac{1}{\Omega_i}\sum_j Z^*_{i,j}\delta\mathbf{u}_{i,j} \quad (1)$$

where Ω_i is the volume of unit cell i and $Z^*_{i,j}$ and $\delta\mathbf{u}_{i,j}$ are the Born effective charge tensor, and relative displacement of j-th atom, respectively. The calculated total polarization, including the in-plane and out-of-plane components, are shown in **Figure 4c**. Near the BFO/TSO interface, $|\mathbf{P}_i|$ is close to the bulk value ~90 μC/cm^2. At the Bi_2O_3/BFO interface, $|\mathbf{P}_i|$ reaches a value as large as ~140 μC/cm^2 and matches the experimental result (~136 μC/cm^2) very well. The out-of-plane polarization (~86 μC/cm^2) is also in reasonable agreement with the experiment (~109 μC/cm^2). It is worthwhile to point out that even the out-of-plane polarization alone is already comparable to the total polarization of bulk BFO and indicates a better ferroelectric property. The strong coupling between the surface monolayer and the polarization of BFO can be attributed to the break of local symmetry and the change of the ionic charge of the Bi atoms at the surface. **Table S1** and **Figure S6** summarize the Bader charge analysis[33] and layer-resolved density of states (DOS) of Bi and O atoms for our simulated structure. Our results show that, although the ionic charge of Bi in BFO is +1.87 (close to the +2 oxidation state), its value at the Bi_2O_3/BFO interface reduces to +1.64 and down to only +1.27 in Bi_2O_3 layer, indicating that the nominally empty Bi 6*p* orbitals become occupied near the surface (see Supporting Information for further details). The lower ionic charge of Bi atoms in Bi_2O_3 weakens the attraction between Bi and O atoms compared to BFO and increases their bond length. Consequently, the imbalance between the weaker Bi-O bond in the vicinity of the surface and the comparatively stronger bond in BFO leads to a strong dipole field, which effectively counteracts the depolarizing field and causes the enhancement in polarization.

The formation of the rumpling *c*-/*a*-type MPB-like domain structure can be explained by incorporating the surface single layer structures into phase-field simulations (see Supporting Information for details). The interaction between the surface layer and BFO film was modeled by applying an effective built-in potential on the surface with the surface monolayer. The result is shown in **Figure 4d**, which qualitatively reproduces the rumpling *c*-type/*a*-type domain structure. The simulated *c*/*a* ratio and $\left|\mathbf{P}_i\right|$ of *c*-type domains are consistent with both experiments and DFT calculations as well (see **Figure S7-S8**). Without such surface layer, the polarization in this ultrathin film would otherwise be substantially suppressed, due to the depolarizing field as well as the surface effect. This is clearly observed at the bottom layers of the film from both phase-field simulation and the experimental data, where the polarization is less affected by the surface layer. Near the surface layers, the polarization is mainly upward, indicating a super tetragonal-like phase. Meanwhile, a polarization component normal to the mapping plane is also found in the simulation and consistent with the strain induced super tetragonal phase[34]. In summary, our DFT and phase-field simulations fully reproduce the key experimental results and reveal a novel polarization enhancing scenario, where a potential enhancement of ultrathin films' ferroelectricity can be realized via the introduction of specific surface structures.

We remark that the unique Bi_2O_{3-x} monolayer observed by our STEM experiments and the enhanced polarization is nontrivial and it might be ubiquitous for BFO films. As a matter of fact, the same surface structures are also observed in 5 nm and 20 nm thick BFO films. With the increase of thickness, their effects become less prominent and hence these films exhibit the conventional 109° domain structures of *R*-phase BFO (see **Figure S4** and **S5**). Nevertheless, the ferroelectricity in the vicinity of the surface layers is still affected. For example, **Figure S4a** displays a map of the *c*/*a* ratio

and $-D_{\mathrm{FB}}^{(z)}$ for a 5 nm BFO film. Similar to the ultrathin 2 nm film, a substantial increase of $-D_{\mathrm{FB}}^{(z)}$ up to ~0.48 Å near the surface is found. Similar phenomena have also been reported in BFO/$La_{0.7}Sr_{0.3}MnO_3$/$SrTiO_3$ thin films by Kim *et al.*[35]. Using STEM, they discovered a sudden increase of displacement (~90-100%) and lattice spacing (~10%) at the surface and these structural anomalies are interpreted as surface dielectric dead layers. The unique MPB-like nanodomain structure and the very large *c*/*a* ratio (~1.2) of the *c*-type domains suggest a possibly very good piezoelectric response property of the ultrathin film because the domain structure is similar to MPB[36] and a change of the overall polarization of the thin film could lead to large strain variations. Therefore, it might be useful to develop high-performance ultrathin piezoelectric response nanodevices. However, in order to exploit these structures to obtain well-controlled enhanced polarization and MPB-like domain structure in the ferroelectric thin films, a very fine control of the surface chemistry is mandatory. A possible route is to combine MBE growth together with electron lithography. Furthermore, it's also worthwhile to note that whether similar polarization enhancement mechanism could be applied to other perovskite ferroelectric materials, e.g. the classical $BaTiO_3$, $Pb(Ti_{1-x}Zr_x)O_3$ systems at the reduced dimension is still an open question and follow-up work is still undergoing. We note that recent work by Fan *et al.*[37] showed that by doping BFO film with Ga, a super-tetragonal-like structure with largely enhanced polarization could be stabilized regardless of film thickness. This finding, along side with our results, could possibly give rise to material systems of far more superior performance.

In conclusion, our combined experimental and theoretical studies clearly demonstrate how an enhancement of ferroelectricity can be achieved in ultrathin ferroelectric films through the engineering of its surface. This is nontrivial because surface relaxation, reconstruction and defects

are very common in a variety of ferroelectric oxides[38–40]. The change of the surface structure will not only introduce lattice disorder and coordination distortion, but also give rise to long-range electrical dipole interactions because of the nature of ionic crystals. As a consequence, instead of being confined only at the surface, unexpected behaviors permeating throughout the whole film could be introduced. For example, a reversible switching of ferroelectric domains can be achieved by controlling the surface chemical potential[41]. In our case, the surface monolayer plays a similar role by introducing effective polarizing fields and leads to the unexpected giant polarizations and MPB-like nanodomains with large variations in *c*/*a* ratios. Our results demonstrate that novel or better physical properties can be exploited and explored by modifying the boundary condition of an ultrathin ferroelectric film's surface. These findings offer a new dimension and route to designing thin film structures and tailoring its properties by means of precise control of local ferroelectricity through the engineering of boundary conditions.

Experimental Section

Materials synthesis and characterization: The $BiFeO_3$ films were grown on single crystal $(1\,\bar{1}0)_O$ $TbScO_3$ substrate by reactive-molecular beam epitaxy (MBE). The 2 nm thick $BiFeO_3$ layer was deposited at a substrate temperature of 625 °C in distilled ozone (~80% ozone) at a partial pressure of 1×10^{-6} Torr. This window was determined for our estimated elemental fluxes of ~2×10^{13} at·cm^{-2}·s^{-1} for Fe and ~1×10^{13} at·cm^{-2}·s^{-1} for Bi as measured on a quartz crystal monitor prior to growth. The 5 nm films and 20 nm films were grown in a similar fashion with a growth temperature determined in the same manner prior to their growth. Cross-sectional TEM samples were prepared by mechanical

polishing followed by argon ion milling. STEM HAADF and EELS experiments were carried out on an FEI Titan 80-300 microscope equipped with double aberration correctors at 300 kV. The accelerating voltage, convergence angle of the incident electrons, and the collection angle for HAADF imaging are 300 kV, 29 mrad and 79-200 mrad, respectively. EELS experiments were performed with the convergence angle, the collection angle and energy dispersion 22 mrad, 36 mrad and 1 eV/channel, respectively. For each pixel, a dwell time of 0.1 s was used to acquire the EEL spectra.

Supporting Information

Supporting Information is available from the Wiley Online Library or from the author.

Acknowledgements

The authors (L.X. & P.W.) would like to acknowledge funding from the National Basic Research Program of China (Grant No. 2015CB654900) and National Natural Science Foundation of China (No. 51302132 & No. 11474147). The work at University of California-Irvine and at University of Michigan was supported by the Department of Energy (DOE) under Grant No. DE-SC0014430 (L.X., L.Z.L., P.G., C.T.N. & X.Q.P.). The work at the Pennsylvania State University is supported by the DOE, Office of Basic Energy Sciences, Division of Materials Science and Engineering, under Grant No. DE-FG02-07ER46417 (F.X. and L.Q.C.) and partially by the NSF under Grant No. DMR-1210588 (Z.H.). This work is also supported partially by NSF MRSEC under Grant No. DMR-1420620 (Y.Z. & F.X.). The work at Cornell University was supported by the U.S. Department of Energy, Office of Basic Energy Sciences, Division of Materials Sciences and Engineering, under Award No. DE-SC0002334 (C.A.H. and D.G.S.). The authors would also like to acknowledge the National Center for Electron Microscopy at Lawrence Berkeley National Laboratory for their support under the DOE Grant No. DE-AC02-05CH11231 for user facilities. This work was performed in part at the Cornell Nanoscale Facility, a member of the National Nanotechnology Infrastructure Network, which is supported by the National Science Foundation (Grant No. ECCS-0335765). This research used resources of the National Energy Research Scientific Computing Center, a DOE Office of Science User Facility supported by the Office of Science of the U.S. Department of Energy under Contract No. DE-AC02-05CH11231 (E.K.). The

authors would like to acknowledge Dr. J.R. Jokisaari, Dr. G.W. Graham, Dr. H.D. Lu and Prof. A. Gruverman for helpful discussions.

Received: ((will be filled in by the editorial staff))
Revised: ((will be filled in by the editorial staff))
Published online: ((will be filled in by the editorial staff))

References

[1] N. A. Spaldin, M. Fiebig, *Science* **2005**, *309*, 391.

[2] M. Dawber, K. M. Rabe, J. F. Scott, *Rev. Mod. Phys.* **2005**, *77*, 1083.

[3] R. Ramesh, N. A. Spaldin, *Nat. Mater.* **2007**, *6*, 21.

[4] J. F. Scott, *Ferroelectric Memories*, Springer-Verlag Berlin Heidelberg, **2000**.

[5] A. Gruverman, A. Kholkin, *Rep. Prog. Phys.* **2006**, *69*, 2443.

[6] N. Setter, D. Damjanovic, L. Eng, G. Fox, S. Gevorgian, S. Hong, A. Kingon, H. Kohlstedt, N. Y. Park, G. B. Stephenson, I. Stolitchnov, A. K. Taganstev, D. V. Taylor, T. Yamada, S. Streiffer, *J. Appl. Phys.* **2006**, *100*, 051606.

[7] Z. Wen, C. Li, D. Wu, A. Li, N. Ming, *Nat. Mater.* **2013**, *12*, 617.

[8] M. E. Lines, A. M. Glass, *Principles and Applications of Ferroelectrics and Related Materials*, OUP Oxford, **2001**.

[9] D. J. Kim, J. Y. Jo, Y. S. Kim, Y. J. Chang, J. S. Lee, J.-G. Yoon, T. K. Song, T. W. Noh, *Phys. Rev. Lett.* **2005**, *95*, 237602.

[10] A. Petraru, H. Kohlstedt, U. Poppe, R. Waser, A. Solbach, U. Klemradt, J. Schubert, W. Zander, N. A. Pertsev, *Appl. Phys. Lett.* **2008**, *93*, 072902.

[11] D. D. Fong, G. B. Stephenson, S. K. Streiffer, J. A. Eastman, O. Auciello, P. H. Fuoss, C. Thompson, *Science* **2004**, *304*, 1650.

[12] H. Béa and S. Fusil and K. Bouzehouane and M. Bibes and M. Sirena and G. Herranz and E. Jacquet and J.-P. Contour and A. Barthélémy, *Jpn. J. Appl. Phys.* **2006**, *45*, L187.

[13] L. Despont, C. Koitzsch, F. Clerc, M. G. Garnier, P. Aebi, C. Lichtensteiger, J.-M. Triscone, F. J. Garcia de Abajo, E. Bousquet, P. Ghosez, *Phys. Rev. B* **2006**, *73*, 094110.

[14] H. Yamada, V. Garcia, S. Fusil, S. Boyn, M. Marinova, A. Gloter, S. Xavier, J. Grollier, E. Jacquet, C. Carrétéro, C. Deranlot, M. Bibes, A. Barthélémy, *ACS Nano* **2013**, *7*, 5385.

[15] M. Stengel, D. Vanderbilt, N. A. Spaldin, *Nat. Mater.* **2009**, *8*, 392.

[16] D. Lee, H. Lu, Y. Gu, S.-Y. Choi, S.-D. Li, S. Ryu, T. R. Paudel, K. Song, E. Mikheev, S. Lee, S. Stemmer, D. A. Tenne, S. H. Oh, E. Y. Tsymbal, X. Wu, L.-Q. Chen, A. Gruverman, C. B. Eom, *Science* **2015**, *349*, 1314.

[17] G. Catalan, J. F. Scott, *Adv. Mater.* **2009**, *21*, 2463.

[18] Y.-H. Chu, L. W. Martin, M. B. Holcomb, R. Ramesh, *Mater. Today* **2007**, *10*, 16.

[19] C. T. Nelson, B. Winchester, Y. Zhang, S.-J. Kim, A. Melville, C. Adamo, C. M. Folkman, S.-H. Baek, C.-B. Eom, D. G. Schlom, L.-Q. Chen, X. Pan, *Nano Lett.* **2011**, *11*, 828.

[20] C. T. Nelson, P. Gao, J. R. Jokisaari, C. Heikes, C. Adamo, A. Melville, S.-H. Baek, C. M. Folkman, B. Winchester, Y. Gu, Y. Liu, K. Zhang, E. Wang, J. Li, L.-Q. Chen, C.-B. Eom, D. G. Schlom, X. Pan, *Science* **2011**, *334*, 968.

[21] L. A. Schmitt, K. A. Schönau, R. Theissmann, H. Fuess, H. Kungl, M. J. Hoffmann, *J. Appl. Phys.* **2007**, *101*, 251911.

[22] R. J. Zeches, M. D. Rossell, J. X. Zhang, A. J. Hatt, Q. He, C.-H. Yang, A. Kumar, C. H. Wang, A. Melville, C. Adamo, G. Sheng, Y.-H. Chu, J. F. Ihlefeld, R. Erni, C. Ederer, V. Gopalan, L. Q. Chen, D. G. Schlom, N. A. Spaldin, L. W. Martin, R. Ramesh, *Science* **2009**, *326*, 977.

[23] C. M. Folkman, S. H. Baek, H. W. Jang, C. B. Eom, C. T. Nelson, X. Q. Pan, Y. L. Li, L. Q. Chen, A. Kumar, V. Gopalan, S. K. Streiffer, *Appl. Phys. Lett.* **2009**, *94*, 251911.

[24] H. Liu, P. Yang, K. Yao, K. P. Ong, P. Wu, J. Wang, *Adv. Funct. Mater.* **2012**, *22*, 937.

[25] S. Hull, S. T. Norberg, M. G. Tucker, S. G. Eriksson, C. E. Mohn, S. Stolen, *Dalton Trans.* **2009**, *40*, 8737.

[26] X. Martí, P. Ferrer, J. Herrero-Albillos, J. Narvaez, V. Holy, N. Barrett, M. Alexe, G. Catalan, *Phys. Rev. Lett.* **2011**, *106*, 236101.

[27] R. Jarrier, X. Marti, J. Herrero-Albillos, P. Ferrer, R. Haumont, P. Gemeiner, G. Geneste, P. Berthet, T. Schülli, P. Cevc, R. Blinc, S. S. Wong, T.-J. Park, M. Alexe, M. A. Carpenter, J. F. Scott, G. Catalan, B. Dkhil, *Phys. Rev. B* **2012**, *85*, 184104.

[28] I. MacLaren, L. Wang, O. Morris, A. Craven, R. Stamps, *APL Mater.* **2013**, *1*, 021102.

[29] I. MacLaren, B. Sala, S. M. L. Andersson, T. J. Pennycook, J. Xiong, Q. X. Jia, E.-M. Choi, J. L. MacManus-Driscoll, *Nanoscale Res. Lett.* **2015**, *10*, 407.

[30] R. D. King-Smith, D. Vanderbilt, *Phys. Rev. B* **1993**, *47*, 1651.

[31] R. D. King-Smith, D. Vanderbilt, *Phys. Rev. B* **1994**, *49*, 5828.

[32] P. Ghosez, J.-P. Michenaud, X. Gonze, *Phys. Rev. B* **1998**, *58*, 6224.

[33] W. Tang, E. Sanville, G. Henkelman, *J. Phys. Condens. Matter* **2009**, *21*, 084204.

[34] Z. Chen, X. Zou, W. Ren, L. You, C. Huang, Y. Yang, P. Yang, J. Wang, T. Sritharan, L. Bellaiche, L. Chen, *Phys. Rev. B* **2012**, *86*, 235125.

[35] Y.-M. Kim, A. N. Morozovska, E. A. Eliseev, A. R. Lupini, Y.-H. Chu, P. Yu, R. Ramesh, S. J. Pennycook, S. V. Kalinin, A. Y. Borisevich, *Microsc. Microanal.* **2013**, *19*, 1928.

[36] R. Guo, L. E. Cross, S.-E. Park, B. Noheda, D. E. Cox, G. Shirane, *Phys. Rev. Lett.* **2000**, *84*, 5423.

[37] Z. Fan, J. Xiao, H. Liu, P. Yang, Q. Ke, W. Ji, K. Yao, K. P. Ong, K. Zeng, J. Wang, *ACS Appl. Mater. Interfaces* **2015**, *7*, 2648.

[38] K. Ishikawa, T. Uemori, *Phys. Rev. B* **1999**, *60*, 11841.

[39] S. Tinte, M. G. Stachiotti, *Phys. Rev. B* **2001**, *64*, 235403.

[40] A. M. Bratkovsky, A. P. Levanyuk, *Phys. Rev. Lett.* **2005**, *94*, 107601.

[41] R. V. Wang, D. D. Fong, F. Jiang, M. J. Highland, P. H. Fuoss, C. Thompson, A. M. Kolpak, J. A. Eastman, S. K. Streiffer, A. M. Rappe, G. B. Stephenson, *Phys. Rev. Lett.* **2009**, *102*, 047601.

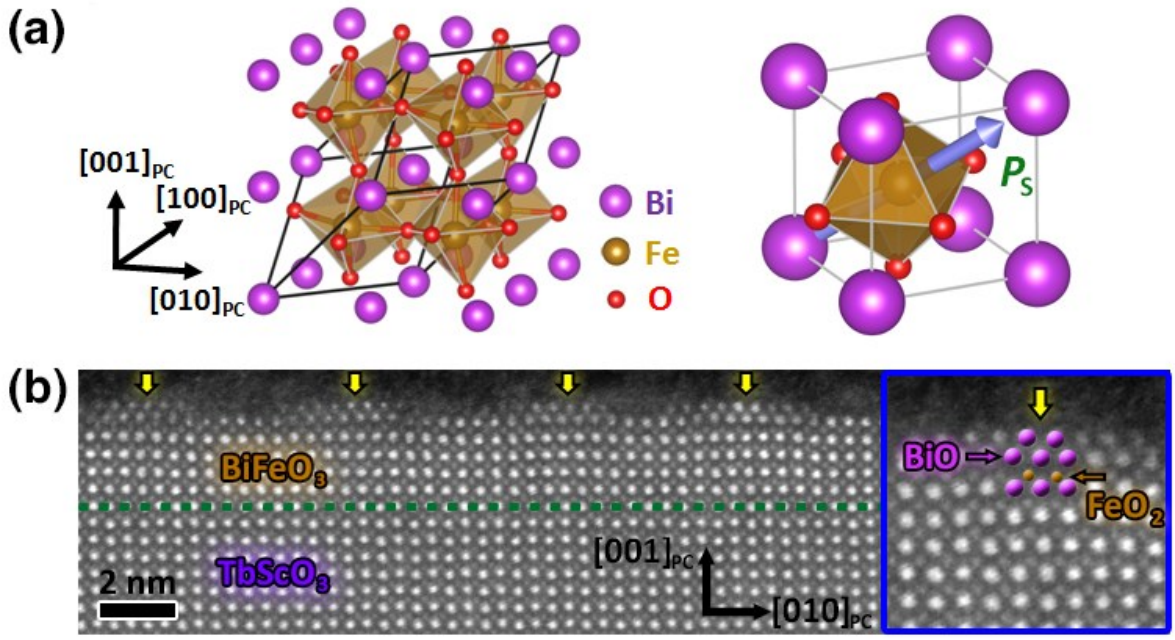

Figure 1. The atomic structure of $BiFeO_3$ and an STEM HAADF image of a 2 nm thick $BiFeO_3$/TbScO3 $(1\,\bar{1}0)_O$ film. a) Schematic structure of the *rhombohedral* phase of $BiFeO_3$. b) Cross-sectional STEM HAADF image of a 2 nm thick $BiFeO_3$/$TbScO_3$ film viewed along the $[100]_{PC}$ zone axis, where the interface is indicated by the green dashed line. The yellow arrows indicate the unique single atomic layers on the surface. For a better view of the surface structure, see the inset for a magnified image.

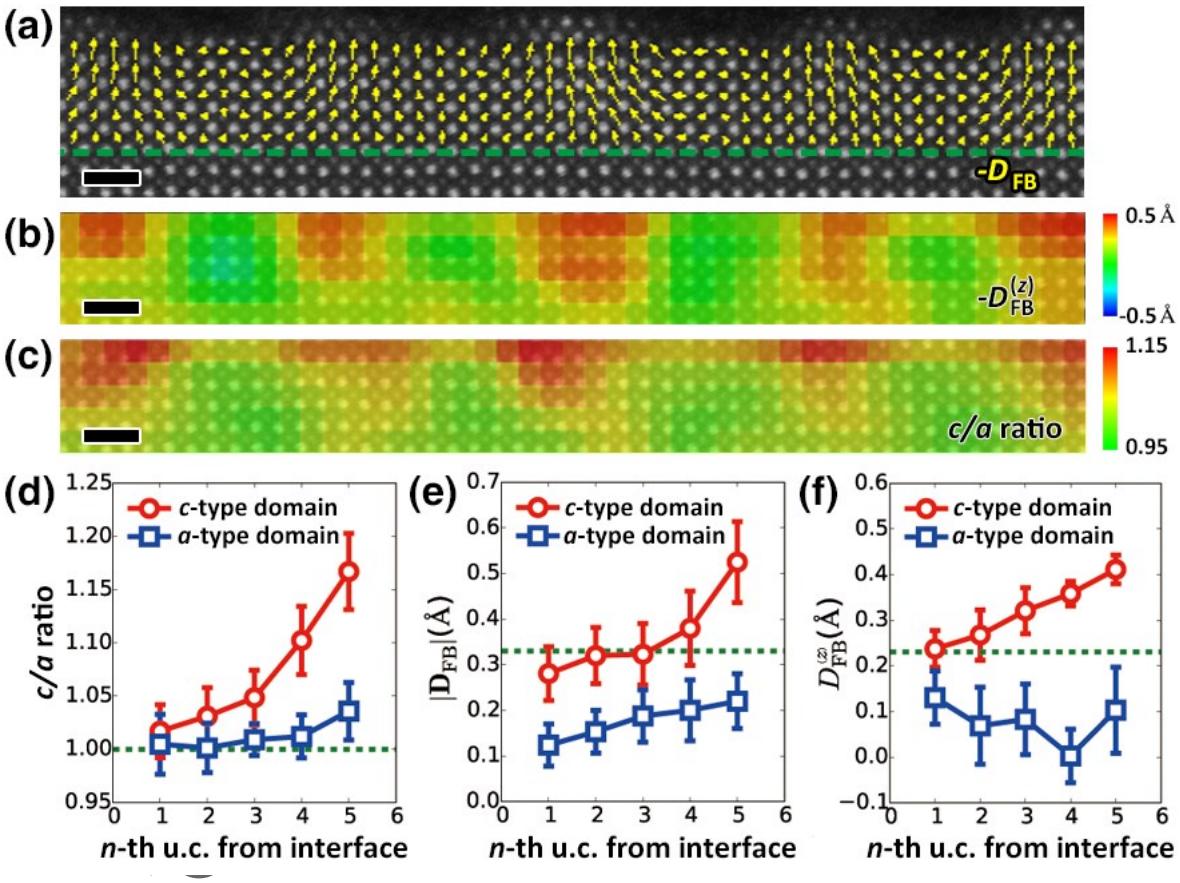

Figure 2. Maps of the ferroelectric polarization and *c*/*a* ratio of the 2 nm thick $BiFeO_3$ film. a) $-\mathbf{D}_{FB}$ map, b) $-D_{FB}^{(z)}$ map, c) *c*/*a* ratio map of the film. The scalebars in (a), (b) & (c) are 1 nm. d) *c*/*a* ratio as a function of distance from the interface, e) $|\mathbf{D}_{FB}|$ and f) $-D_{FB}^{(z)}$ of *c*-/*a*-type domains. The green dash lines in (d), (e) & (f) indicate the *c*/*a* ratio, $|\mathbf{D}_{FB}|$ and $-D_{FB}^{(z)}$ of bulk $BiFeO_3$, respectively.

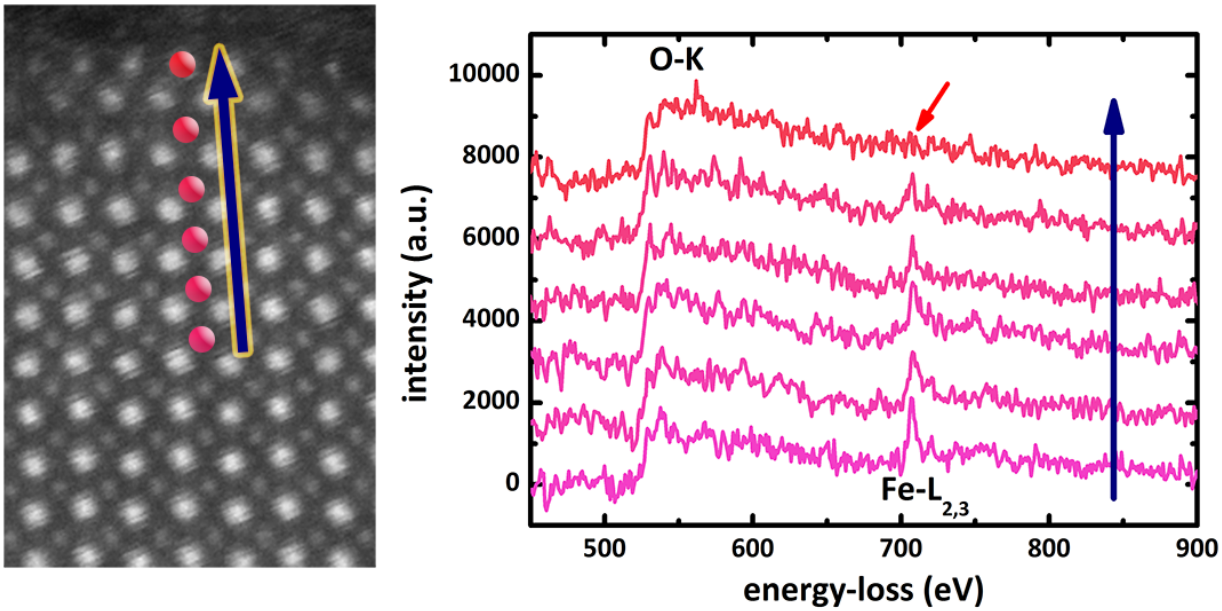

Figure 3. Line scan profile of Fe-$L_{2,3}$ and O-K energy-loss spectra. The position of each EELS spectrum (from bottom to top) is indicated by the circles in the left panel and the corresponding spectrum is shown in the right panel from bottom to top. As is indicated by the red arrow, the energy-loss peak of Fe-$L_{2,3}$ (~708 eV) vanishes at the surface layer, while that of O-K changes much less through the film.

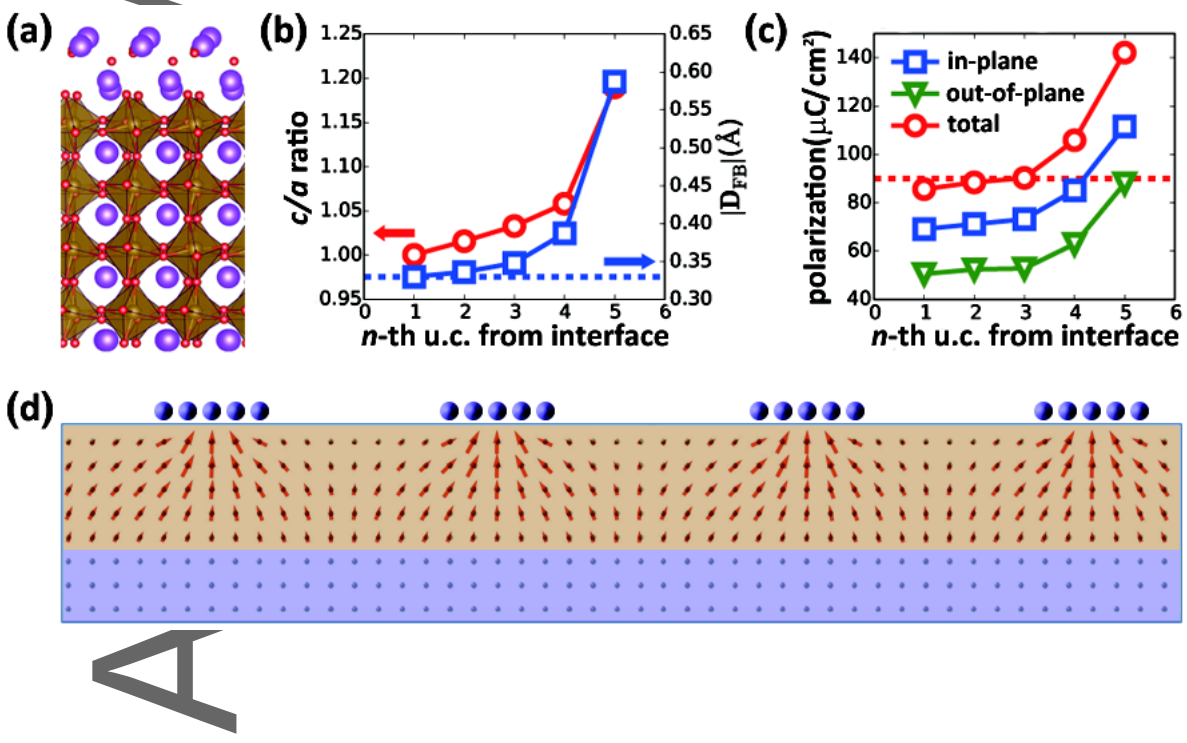

Figure 4. DFT and phase-field calculation results of ultrathin $BiFeO_3$ film with a single atomic Bi_2O_3 layer on the surface. a) atomic structure after structural relaxation, b) *c*/*a* ratio, $\left|\mathbf{D}_{\mathrm{FB}}\right|$ and, c) ferroelectric polarization by DFT. The blue and red dash lines indicate $\left|\mathbf{D}_{\mathrm{FB}}\right|$ and total polarization of bulk $BiFeO_3$, respectively. d) Phase-field simulation results.

A giant enhancement of ferroelectric polarization in ultrathin 2 nm $BiFeO_3$ film is reported. With the addition of a Bi_2O_{3-x} monolayer on the surface of ferroelectric $BiFeO_3$ thin films, the ferroelectric polarization of the ultrathin 2 nm $BiFeO_3$ film is stabilized and dramatically increased up to ~150 $\mu C/cm^2$, demonstrating the possibility to enhance the performance of ferroelectric materials at the reduced dimension.

Keywords: ultrathin ferroelectric film, polarization enhancement, surface effect, domain structure, scanning transmission electron microscopy

*Lin Xie, Linze Li, Colin A. Heikes, Zijian Hong, Peng Gao, Christopher T. Nelson, Fei Xue, Emmanouil Kioupakis, Longqing Chen, Darrel G. Schlom, Peng Wang, Xiaoqing Pan**

Giant Ferroelectric Polarization in Ultrathin Ferroelectrics via Boundary-condition Engineering

ToC Figure

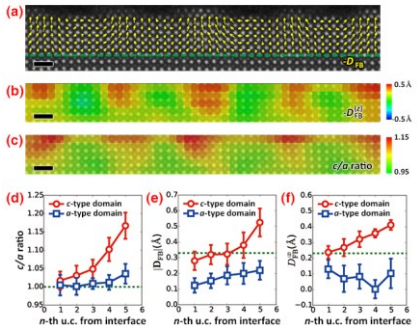

Supporting Information

Giant Ferroelectric Polarization in Ultrathin Ferroelectrics via Boundary-condition Engineering

*Lin Xie, Linze Li, Colin A. Heikes, Yi Zhang, Zijian Hong, Peng Gao, Christopher T. Nelson, Xue Fei, Emmanouil Kioupakis, Longqing Chen, Darrel G. Schlom, Peng Wang, Xiaoqing Pan**

1. Polar displacement mapping

Atomic polar displacements $\mathbf{D}_{\mathrm{FB}}$ were directly measured from the STEM HAADF image by fitting the image with a series of two-dimensional (2D) Gaussian functions[S1]. After fitting, the atomic

positions are extracted from the centers of these 2D Gaussian functions. $\mathbf{D}_{FB}$ is defined as the off-center displacement of the central *B*-site Fe atoms with respect to the center of four surrounding *A*-site Bi atoms. It is well accepted that the polarization of BFO is essentially due to the relative displacements between Bi and O atoms[S2]. Hence the relative displacement between Fe and Bi, $\mathbf{D}_{FB}$, is in the opposite direction of the actual polarization and its value is proportional to the polarization.

2. Atomic structure of Bi_2O_3

Figure S1a displays the schematic atomic structure of Bi_2O_3[25]. The lattice parameters of Bi_2O_3 are a=b=7.7439 Å, c=5.6287 Å, α=β=γ=90°, respectively. It can be readily found that the lattice of Bi_2O_3 is compatible with $TbScO_3$'s $[110]_O$×$[001]_O$ basis (~7.918 Å). **Figure S1b** displays the projected atomic structure of Bi_2O_3 viewed along [110] zone axis and the zigzag structure of Bi atoms on [001] plane can be clearly observed. This zigzag structure is in good agreement with the experiment observations (Figure 1b) and DFT calculation results (Figure 4a).

3. Detailed studies of surface monolayers in 2 nm/5 nm/20 nm $BiFeO_3$/$TbScO_3$ $(1\bar{1}0)_O$ films

The ultrathin 2 nm film was characterized along the $[010]_{PC}$ direction and **Figure S2** shows the STEM HAADF image. Similar to the surface monolayer structure observed along $[100]_{PC}$ direction (Figure 1b), characteristic discontinuous surface monolayer could also be identified along the

orthogonal $[010]_{PC}$ direction. Combining the structural information from these two orthogonal directions, it is suggested that these monolayers are actually discontinuously distributed on the film's surface, forming two-dimensional islands.

To gain a further understanding of the surface structure, STEM HAADF image simulation was carried out using our home-made multislice image simulation package. The atomic model for simulation was directly taken from the relaxed structure by DFT calculation and the occupancies of surface Bi_2O_3 monolayer are fixed to 50%. The parameters for the STEM imaging conditions are V=300 kV, C_3=10 nm, Δf=Scherzer defocus, C_C=1.5 mm, ΔE=0.7 eV with a convergence angle of 22 mrad. The sample thickness for simulation is 16 nm. Surface thermal-vibrations induced thermal diffuse scatterings were accounted for by specifying different Debye-Waller factors for the atoms on each different site. For BFO film, their Debye-Waller factors were taken from empirical functions (B_{Bi}=1.169, B_{Fe}=0.3106, B_O=0.7875) according to Ref. [S3]. For the Bi atoms on the surface and the subsurface, their Debye-Waller factors were set to 1.636 and 1.403, about 40% and 20% increase with respect to that of the bulk. We note that the exact values of Debye-Waller factors for the surface atoms and even for the whole structure are somewhat arbitrarary because they depend on a number of factors, for example, crystal structure and bond strength. Thus our simulation only offers a qualitative understanding of the structure. **Figure S3** displays the simulated results without and with thermal diffuse scatterings, respectively. For a better comparison, the simulated image intensity I is normalized by its maximum and minimum as:

$$I_{\text{norm}} = \frac{I}{I_{\max} - I_{\min}} \quad \text{(S1)}$$

As is shown in **Figure S3a** and **S3d**, the contrast of the surface monolayer is considerably lower than that of the subsurface and the inner BiO layers due to its relatively lower atomic densities. If thermal diffuse scattering is taken into consideration, the contrast of the surface monolayer is further reduced due to a weaker channeling of electrons along the atomic columns on the surface. These results are qualitatively in agreement with our experimental findings, suggesting a formation of two-dimensional island-like monolayer structures on BFO film.

In order to testify the hypothese that the surface monolayer is probably a transient state during growth, a sequence of BFO/TSO films with thicknesses of 5 nm and 20 nm were grown and their structure were characterized by atomic-resolution STEM HAADF imaging as well. As are shown in **Figure S4** and **Figure S5**, the characteristic single atomic layer can be clearly observed on the surface of the 5 nm and 20 nm films (indicated by yellow arrows in **Figure S4a** and **S5b**), implying that these surface monolayers are ubiquitous in BFO films and might act as nucleation sites during the growth. If more FeO_2 is added, these peculiar surface structures would absorb FeO_2 and transit into proper BFO layers. In analogue to the ultrathin 2 nm thick film, $-\mathbf{D}_{\mathrm{FB}}$, $-D_{\mathrm{FB}}^{(z)}$ and *c*/*a* ratio are measured for the 5 nm thick film and the results are given in **Figure S4b-S4e**. Although the domain structure of the 5 nm thick film is of the conventional 109° domain configuration for *R*-phase BFO, its ferroelectricity in the vicinity of the surface is substantially affected by the surface layers. As shown in Figure S4b and S4e, $-D_{\mathrm{FB}}^{(z)}$ increases rapidly in the vicinity of the surface and reaches about ~0.48 Å at the top surface. Meanwhile, a substantial increase of *c*/*a* ratio is also discovered. These findings are identical to those for the 2 nm thick film. Similar surface structure can also be identified in the 20 nm thick film. **Figure S5a** shows the dark-field image of the 20 nm film and the corresponding atomic-resolution STEM HAADF image is given in **Figure S5b**, in which the same surface structure can also be

found (as indicated by yellow arrows). The polarization in the middle of the 20 nm thick film are mapped and the results are given in **Figure S5c**, where polarization is mainly along <111>$_{PC}$ directions and domains are separated by a 109° domain wall.

4. DFT calculation of ultrathin $BiFeO_3$ film with surface Bi_2O_3

DFT calculations were carried out using Vienna Ab-initio Software Package (VASP)[S4] within the framework of PAW[S5,S6] and LSDA+U[S7]. A symmetrical slab consisting of 5 layers of BiO planes and 5 layers of FeO_2 planes was built on top of 6 unit cells of $TbScO_3$ $(1\,\bar{1}0)_O$. The supercell was chosen to be $\sqrt{2}\times\sqrt{2}$ of the perovskite pseudocubic unit cell and the in-plane lattice constant was fixed to the experimental value of TSO (*a*=5.47 Å, *b*=5.73 Å). The *k*-points were sampled using a 5×5×1 Monkhorst-Pack mesh[S8], the planewave cut-off energy set to 500 eV and *U* and *J* parameters were chosen as U_{eff}=*U*-*J*=2 eV[S2]. To avoid spurious electric fields due to the slab configuration, a 15 Å vacuum region was used to separate the periodic slabs, and the dipole correction was turned on during the calculation. A larger vacuum separation of 20 Å was tested as well and the total energy difference was only ~1 meV. The system is first relaxed by the force criterion (<0.005 eV/Å), which reproduces the rhombohedral ferroelectric phase and *G*-type antiferromagnetic ground state of BFO. After the structure relaxation, a stoichiometric single atomic Bi_2O_3 layer was added on top of the relaxed BFO slab and further relaxations were performed until the maximum force is <0.005 eV/Å. The relaxed structure is insulating.

The Born effective charges (BEC) were calculated by finite difference of Berry-phase polarizations[S9,S10]. The calculated BECs are +4.56, +3.3 and -2.62 for Bi, Fe and O atoms, respectively.

5. Phase-field simulations

In the phase-field simulations, two sets of order parameters are considered, namely spontaneous polarization P_i (i=1, 2, 3) and spontaneous oxygen octahedral rotation θ_i (i=1, 2, 3). The evolution of order parameters are governed by the time-dependent Ginzburg-Landau (TDGL) equations:

$$\frac{\partial P_i(\vec{r},t)}{\partial t} = -L_1 \frac{\delta F}{\delta P_i(\vec{r},t)} \quad (i=1, 2, 3) \tag{S2}$$

$$\frac{\partial \theta_i(\vec{r},t)}{\partial t} = -L_2 \frac{\delta F}{\delta \theta_i(\vec{r},t)} \quad (i=1, 2, 3) \tag{S3}$$

where $\vec{r}$ is the spatial position vector, t is the evolution time step, L_1 and L_2 are the kinetic coefficients for polarization and octahedral rotation, respectively. F is the free energy of the system which is the volume integration of Landau, elastic, electric and gradient energy densities:

$$F = \int \left(f_{\text{Landau}} + f_{\text{elastic}} + f_{\text{electric}} + f_{\text{gradient}} \right) \mathrm{d}V \tag{S4}$$

The bulk Landau energy density has the contribution from polarization and octahedral rotation, namely:

$$f_{\text{Landau}} = f_{\text{polarization}} + f_{\text{rotation}} \quad \text{(S5)}$$

Detailed expressions of the energy density as well as method of solving the phase-field equations can be found in literatures[S11–S14]. All the parameters are taken from literatures[S14,S15]. A quasi-2D simulation with system size of $64\Delta x \times 4\Delta y \times 25\Delta z$ is performed. The grid spacing is chosen as 0.4 nm, i.e., $\Delta x = \Delta y = \Delta z = 0.4$ nm. The system consists of 10 grids of substrate layer, 5 grids of $BiFeO_3$ and 10 grids of air from the bottom to the top along the thickness direction. Mixed electric boundary condition is used, where the dielectric displacement is zero at the bottom of the film and fixed electric potential at the film top. A bias of -1.3V is added at specific location on top of the film to simulate the effective polarizing field induced by the Bi_2O_3 layer[S16], whereas the bias at all the other top areas are fixed to zero to account for the charge compensation from air. Periodic boundary condition is assumed along the in-plane dimensions (*x* and *y* dimensions), while a superposition spectral method is used along *z* direction[S13]. Besides the above structure, in order to accurately treat the open-circuit boundary condition, that is, without charge compensation at the surface, a structure model without surface layers was also calculated in the phase-field simulation.

References

[S1] C. T. Nelson, B. Winchester, Y. Zhang, S.-J. Kim, A. Melville, C. Adamo, C. M. Folkman, S.-H. Baek, C.-B. Eom, D. G. Schlom, L.-Q. Chen, X. Pan, *Nano Lett.* **2011**, *11*, 828.

[S2] J. B. Neaton, C. Ederer, U. V. Waghmare, N. A. Spaldin, K. M. Rabe, *Phys. Rev. B* **2005**, *71*, 014113.

[S3] L. M. Peng, G. Ren, S. L. Dudarev, M. J. Whelan, *Acta Cryst. A* **1996**, *52*, 456.

[S4] G. Kresse, J. Furthmüller, *Phys. Rev. B* **1996**, *54*, 11169.

[S5] P. E. Blöchl, *Phys. Rev. B* **1994**, *50*, 17953.

[S6] G. Kresse, D. Joubert, *Phys. Rev. B* **1999**, *59*, 1758.

[S7] S. L. Dudarev, G. A. Botton, S. Y. Savrasov, C. J. Humphreys, A. P. Sutton, *Phys. Rev. B* **1998**, *57*, 1505.

[S8] H. J. Monkhorst, J. D. Pack, *Phys. Rev. B* **1976**, *13*, 5188.

[S9] R. D. King-Smith, D. Vanderbilt, *Phys. Rev. B* **1993**, *47*, 1651.

[S10] R. D. King-Smith, D. Vanderbilt, *Phys. Rev. B* **1994**, *49*, 5828.

[S11] Y. Li, S. Hu, Z. Liu, L. Chen, *Acta Mater.* **2002**, *50*, 395.

[S12] Y. L. Li, S. Y. Hu, Z. K. Liu, L. Q. Chen, *Appl. Phys. Lett.* **2002**, *81*, 427.

[S13] L. Chen, J. Shen, *Comput. Phys. Commun.* **1998**, *108*, 147.

[S14] F. Xue, Y. Gu, L. Liang, Y. Wang, L.-Q. Chen, *Phys. Rev. B* **2014**, *90*, 220101.

[S15] Q. Li, Y. Cao, P. Yu, R. K. Vasudevan, N. Laanait, A. Tselev, F. Xue, L. Q. Chen, P. Maksymovych, S. V. Kalinin, N. Balke, *Nat. Commun.* **2015**, *6*, 8985.

[S16] Q. Miao, M. Zeng, Z. Zhang, X. Lu, J. Dai, X. Gao, J.-M. Liu, *Appl. Phys. Lett.* **2014**, *104*, 182903.

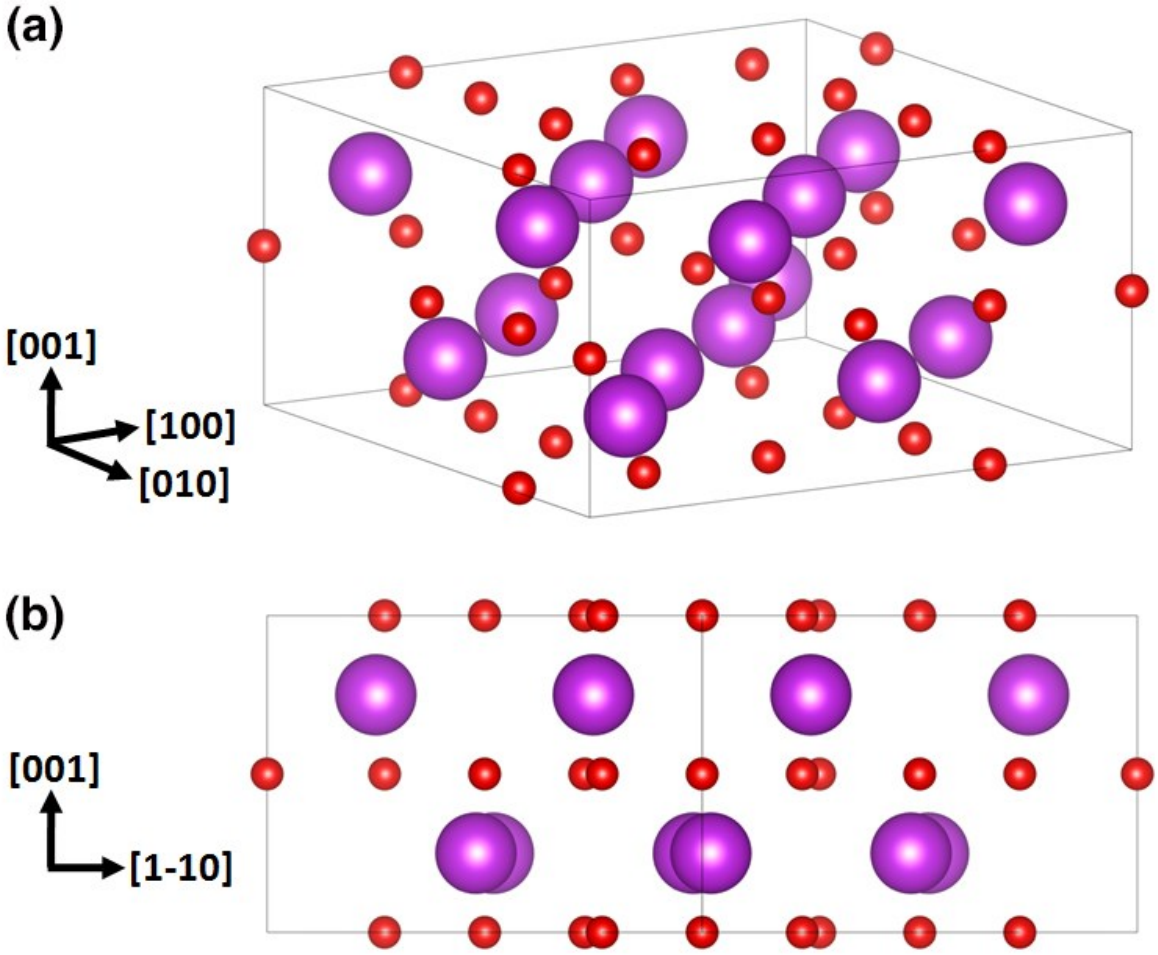

Figure S1. Schematic structure of Bi_2O_3. a) Atomic structure of Bi_2O_3 and b) projection view of Bi_2O_3 along [110] direction. For each Bi_2O_3 atomic layer, its structure has a good match of the BiO plane of $BiFeO_3$ and the stacking of a single Bi_2O_3 layer on BiO plane is similar to a natural stacking of Bi_2O_3 layers along [001] direction.

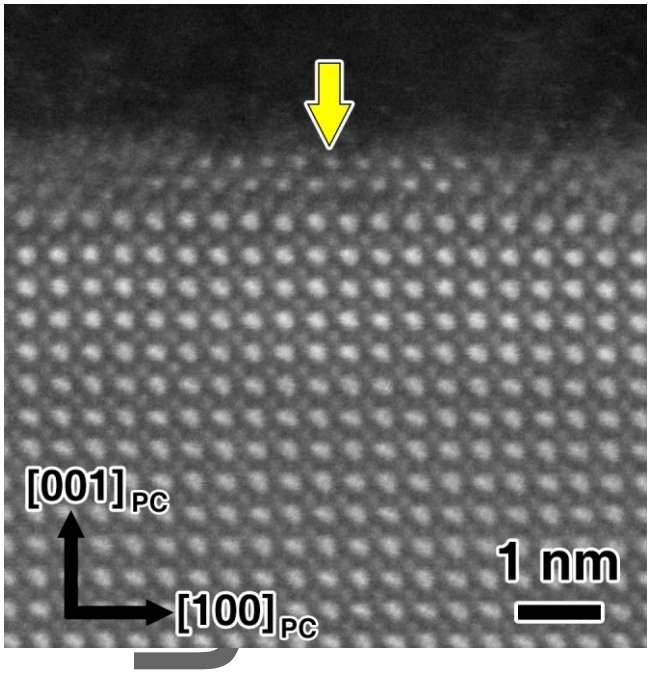

Figure S2. STEM HAADF image of a 2 nm thick $BiFeO_3/TbScO3$ $(1\bar{1}0)_O$ film viewed along the orthogonal $[010]_{PC}$ direction. The surface Bi_2O_{3-x} monolayer can be clearly seen and is indicated by the yellow arrow.

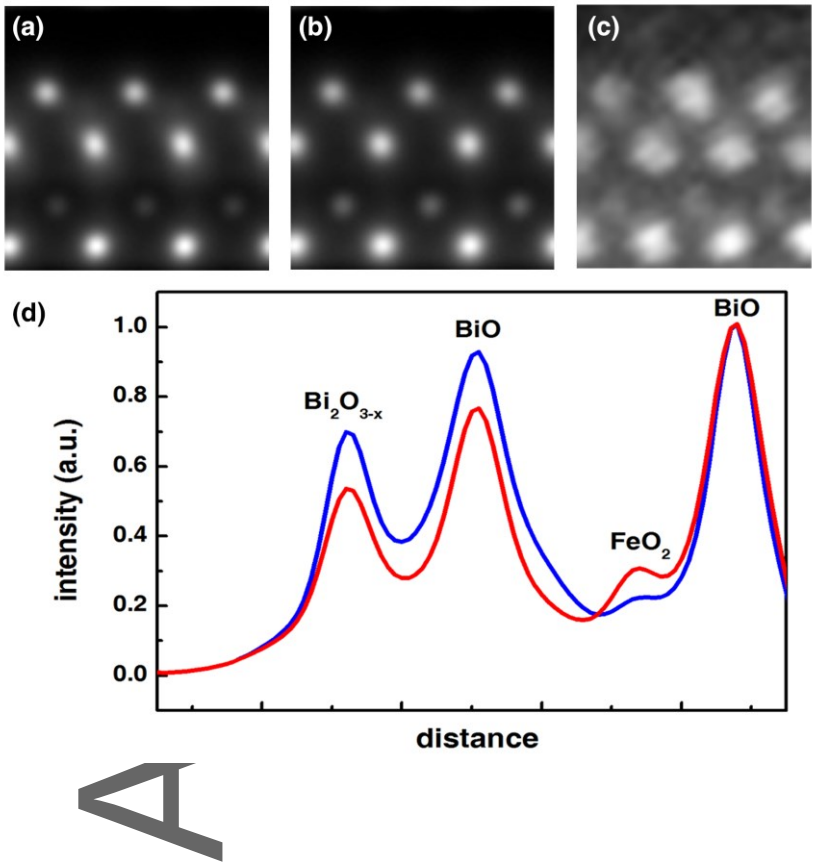

Figure S3. STEM HAADF image simulation results. (a) Simulated image without thermal diffuse scattering. (b) Simulated image with thermal diffuse scattering. (c) Experimental image. (d) Normalized integrated intensity profile along the film's normal direction. The blue and red curves correspond to the calculation results without and with thermal diffuse scatterings, respectively. The contrast of surface monolayer and subsurface BiO layer is substantially reduced with respect to the inner BiO layers due to the island-like structures and surface thermal-vibrations.

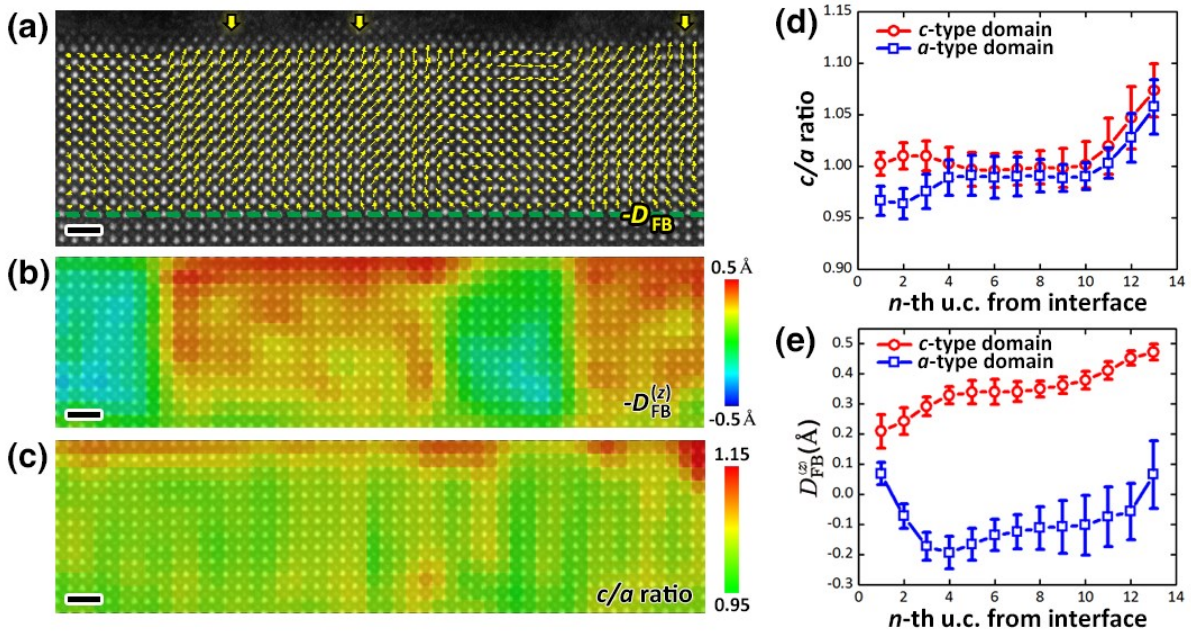

Figure S4. Polarization mapping of 5 nm $BiFeO_3/TbScO_3$ thin film. a) STEM HAADF image and $-\mathbf{D}_{FB}$ mapping of a 5 nm thick $BiFeO_3/TbScO_3$ film viewed along the $[100]_{PC}$ zone axis, where the interface is indicated by the green dashed line. The surface monolayers are indicated by yellow arrows. b) $-D_{FB}^{(z)}$ mapping, c) *c*/*a* ratio mapping of the film. The scalebars in (a)-(c) are 1 nm. d) Quantified *c*/*a* ratio and e) $-D_{FB}^{(z)}$ of *c*-/*a*-type domains.

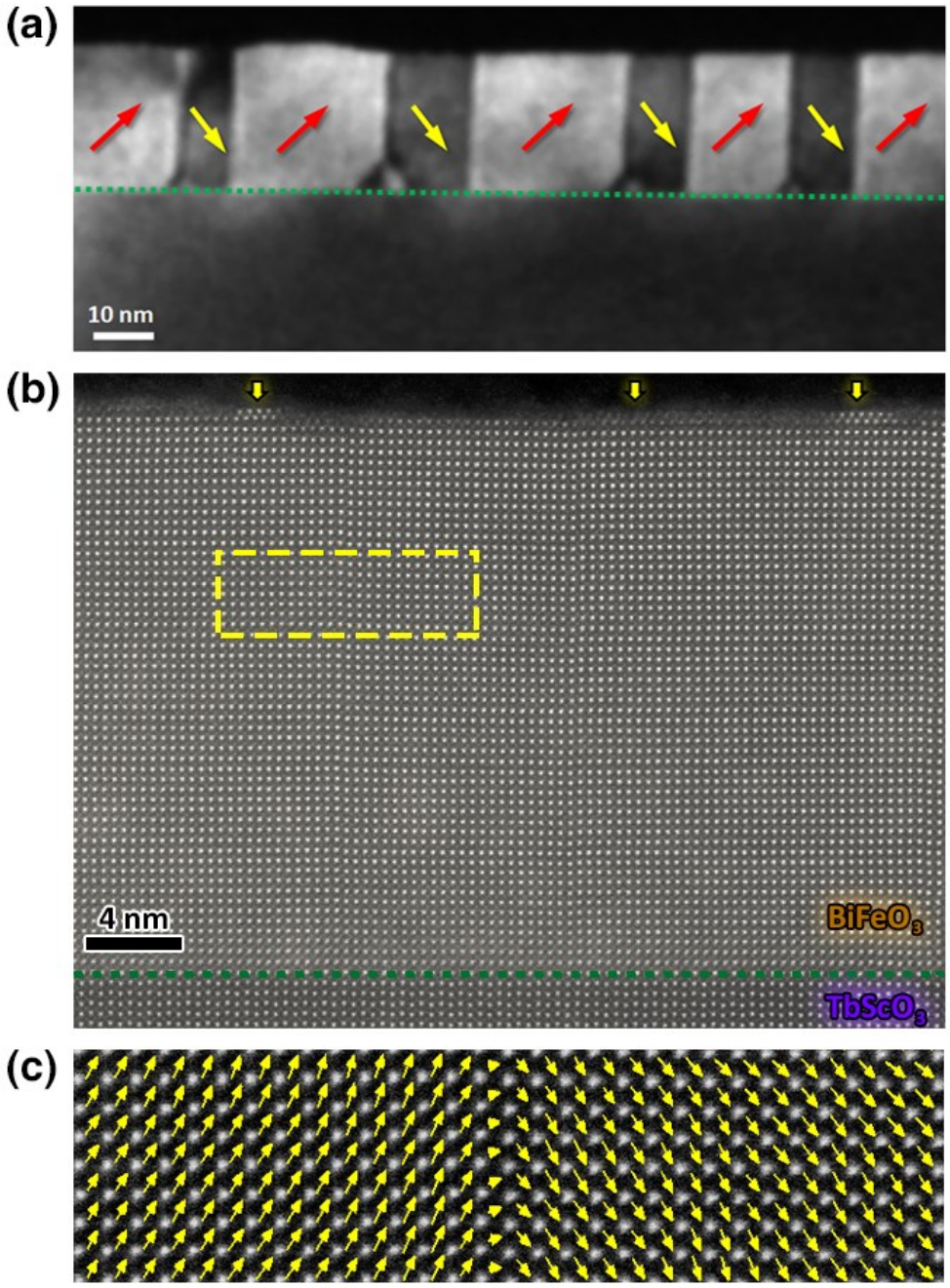

Figure S5. Dark-field and STEM HAADF images of 20 nm $BiFeO_3/TbScO_3$ thin film. a) Dark-field image of a 20 nm thick $BiFeO_3/TbScO_3$ $(1\bar{1}0)_O$ film, in which the interface is indicated by the green dashed line. The red and yellow arrows indicate the polarization of each domain. b) Cross-sectional STEM HAADF image of same film viewed along the

$[100]_{PC}$ zone axis; the interface is indicated by the green dashed line. The yellow arrows indicate the surface monolayers. c) $-\mathbf{D}_{FB}$ mapping of the film.

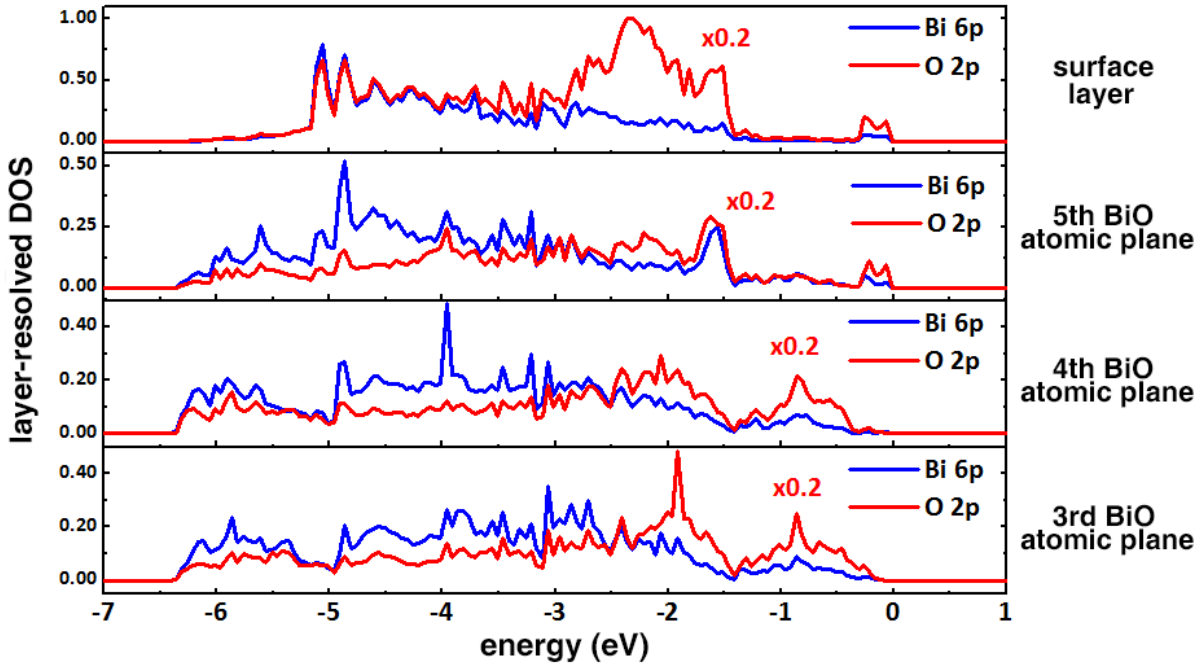

Figure S6. Layer-resolved density of states of Bi 6*p* and O 2*p* electrons in each atomic layer. The Fermi energy is placed at 0 eV and the density of states of O 2*p* electrons is ×0.2 for a better scale. In the surface layer and 5th BiO atomic plane, an overlap of local density of states between Bi 6*p* and O 2*p* orbitals in an energy range from -0.3 eV to 0 eV can be identified.

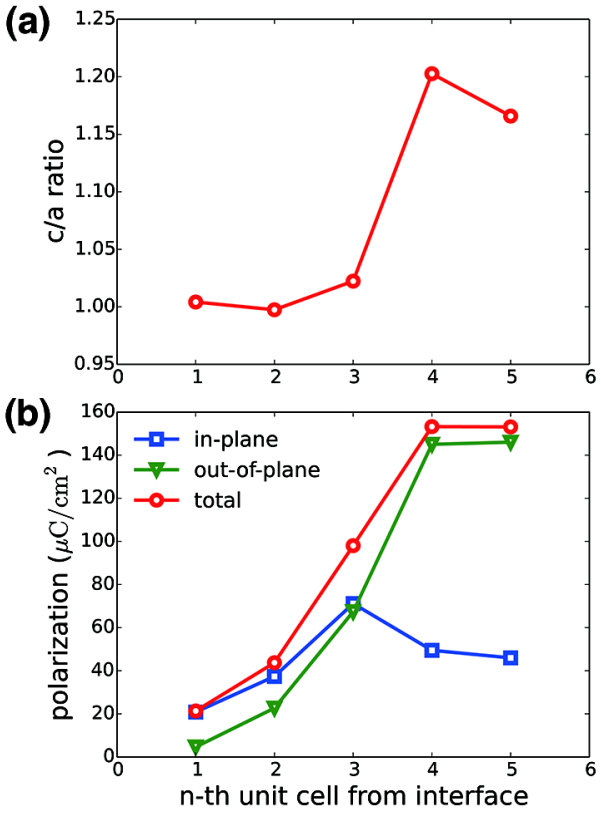

Figure S7. Phase-field simulation results for $BiFeO_3$ film with surface layer. a) *c*/*a* ratio and b) ferroelectric polarization from interface to surface.

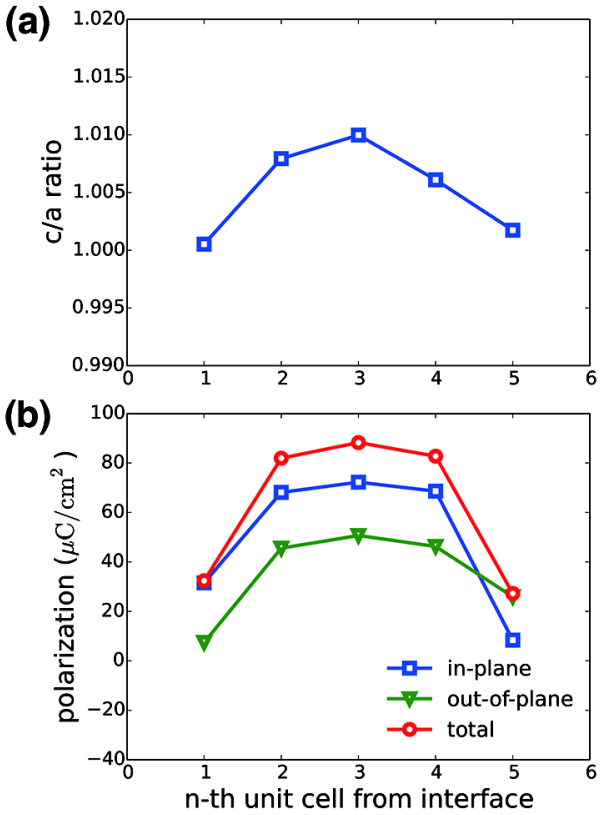

Figure S8. Phase-field simulation results of $BiFeO_3$ film without surface layer. a) *c*/*a* ratio and b) ferroelectric polarization from interface to surface.

	Bi	Fe	O
surface Bi_2O_3 layer	+1.27	-	-1.14
1st BiO layer	+1.64	-	-1.16
1st FeO_2 layer	-	+2.72	-1.18
2nd BiO layer	+1.87	-	-1.20
2nd FeO_2 layer	-	+2.70	-1.19
3rd BiO layer	+1.87	-	-1.19
3rd FeO_2 layer	-	+2.70	-1.19
4th BiO layer	+1.87	-	-1.19

4th FeO_2 layer	-	+2.70	-1.19
5th BiO layer	+1.87	-	-1.19
5th FeO_2 layer	-	+2.70	-1.19

Table S1. Bader charge analysis results of BFO film and surface Bi_2O_3 monolayer. The Bi and O atoms at the surface have relatively lower oxidation state, while the oxidation state of Fe atoms is less affected. Into BFO film, the Bader charge of Bi, Fe and O atoms quickly converges to their bulk values.